PNAS
www.pnas.org

Supplementary Information for

Dronc-independent basal executioner caspase activity sustains *Drosophila* imaginal tissue growth

Natsuki Shinoda, Nozomi Hanawa, Takahiro Chihara, Akiko Koto, and Masayuki Miura

Masayuki Miura
Email: miura@mol.f.u-tokyo.ac.jp

This PDF file includes:

www.pnas.org/cgi/doi/10.1073/pnas.1904647116

SI Discussion

Dronc-independent regulation of basal executioner caspase activity. Most of the observed caspase activation in both apoptosis and caspase-dependent non-lethal cellular processes (CDPs) in *Drosophila* are acquired via Dronc. However, as several reports have shown, executioner caspase-6 can be activated via self-cleavage (1–3). Thus, it is presumable that *Drosophila* executioner caspases could be activated to a certain extent to conduct non-destructive caspase activation at basal level in the absence of the initiator caspase. From our screening study with *UAS-Dcr2*, we found that *strica* RNAi showed curly-up wing phenotype without showing opaque wing phenotype (SI Appendix, Fig. S7B). Strica is known to activate executioner caspases in the wing imaginal disc (WD) (4). Of note, we identified *strica* as one of the differentially up-regulated genes upon caspase-inhibition in our microarray analysis (SI Appendix, Fig. S11C). Strica might act as a weak activation platform for sustaining basal executioner caspase activity. Thus, identifying the differences between the two initiator caspases of Dronc and Strica is important for future research. We showed that *diap-1*, an E3 ligase against caspase, heterozygous mutant (th^4/+) exhibited increased wing size possibly because of increased basal caspase activity. It is likely that post-translational modifications of caspase proteins are important in regulating basal caspase activity; for examples, Inhibitors of Apoptosis Protein mediates ubiquitination of Dronc via both degradation and non-degradation (5), S-nitrosylation in caspase-3 (6), and phosphorylation in caspase-9 (7). Cellular metabolic status also regulates caspase activation via post-translational modifications (8, 9). Such post-translational modifications (reviewed in (10)) could also contribute to the regulation of basal caspase activity.

Wing size regulation by stabilized Acinus (Acn). The mechanism through which stabilized Acn reduces wing size could not be determined in this study. In *Drosophila*, Acn is reported as a nuclear protein that regulates alternative splicing (11) and basal autophagy (12). Caspase-mediated cleavage of Acn affects various physiological processes, including neurodegeneration and aging (13). Given that the WD is spared from starvation-induced autophagy (14) and that genetically induced autophagy through the overexpression of *atg1* in the WD suppresses growth and even induces apoptosis (15), it is important to properly suppress basal autophagy to accelerate tissue growth. It is also possible that other functions of Acn, such as regulation of alternative splicing, are important in wing size regulation.

SI Materials and Methods

Fly strains and rearing conditions. We raised the flies in standard *Drosophila* medium at 25 °C. For TurboID-mediated biotin labeling experiments, we raised flies in 100 μM biotin containing standard *Drosophila* medium at 25 °C. The following fly strains were used in this study: *C10-Gal4* (gift from E. Hafen), *UAS-GFP* on 3rd chr. (BL1522; SI Appendix, Fig. S1, Fig. S8A-G), *UAS-LacZ* (gift from C. Goodman), *UAS-Dronc*^{DN} (gift from H. Richardson), *UAS-p35* (gift from B. Hay), *UAS-miRHG* (gift from C-H. Cheng), *UAS-GFP* on 2nd chr. (BL1521; Fig. 1G-G'', SI Appendix, Fig. S11), *WP-Gal4* (BL49828), *UAS-mCD8::GFP* (BL5130), *UAS-Dcr2* (BL24651), *th*^{4} (BL5053), *UAS-InR*^{DN} (BL8253), *apterous-Gal4* (BL3041), *UAS-mCD8::GFP* (BL5131), *UAS-dark-RNAi* (V100405), *UAS-mCD8::PARP::VENUS* (16), *Actin5C-Gal4* (BL4414), *UAS-SCAT3*^{DEVD} (17), *UAS-SCAT3*^{DEVG} (18), *dronc*^{AA8} (19), *dcp-1::V5::TurboID*, *drice::V5::TurboID* and, *dronc::V5::TurboID* (generated in this study; details are given below), *Def(2R)ED1200/SM6a* (Kyoto150404), *acn*^{27}*/CyO*; *acnP-myc-Acn*^{WT}*/TM6B*, *acn*^{27}*/CyO*; *acnP-myc-Acn*^{D527A}*/TM6B* (gift from H. Krämer). The caspase-RNAi lines used for the screening are as follows: *UAS-dronc-RNAi* (includes BL32963, V23033, V23035), *UAS-dredd-RNAi* (includes BL34070, V28041), *UAS-strica-RNAi* (includes BL54059, V22593, V22594), *UAS-drice-RNAi* (includes BL32403, V28064, V28065), *UAS-dcp-1-RNAi* (includes BL28909, BL38315, V34328, V34330, V107560), *UAS-decay-RNAi* (includes BL65879, V43028, V43029, V100168), and *UAS-damm-RNAi* (includes BL63622, V330204). Autophagy-related gene-RNAi lines used for the screening are as follows: *UAS-atg3-RNAi* (V101364, gift from G. Juhasz), *UAS-atg18a-RNAi* (BL28061, gift from G. Juhasz), *UAS-atg7-RNAi* (V27432, V45558, V45560, V45561), *UAS-atg9-RNAi* (V10045, V330100), and *UAS-atg13-RNAi* (V27955, V27956). BL: Bloomington Drosophila Stock Center, V: Vienna Drosophila Resource Center.

Generation of *caspase::V5::TurboID* knock-in alleles using CRISPR/Cas9. *V5::TurboID* was inserted at the 3′ end of caspase-coding sequences (*dcp-1, drice,* and *dronc*) to generate *caspase::V5::TurboID* knock-in alleles (schemes in Fig. 5A-C) through CRISPR/Cas9-mediated homology-directed repair. Pairs of guide RNAs were identified using CRISPR Optimal Target Finder tool available on flyCRISPR (http://flycrispr.molbio.wisc.edu/). The DNA fragments for the guide RNAs were subcloned in the BbsI-digested U6b-sgRNA-short vector ((20); gift from N. Perrimon). The following primers were annealed to generate the DNA fragments for guide RNAs: *Dcp-1::V5::TurboID-1* (5′-TTCGGGTGGCCATACTCTCGCACG-3′ and 5′-AAACCGTGCGAGAGTATGGCCACC-3′), *Dcp-1::V5::TurboID-2* (5′-TTCGGGAAGCGGGGCAGTTTGGAG-3′ and 5′-AAACGGGTGCAGGACTCAAAGTCC-3′), *Drice::V5::TurboID-1* (5′-TTCGGGACTTTGAGTCCTGCACCC-3′ and 5′-AAACCGTGCGAGAGTATGGCCACC-3′), *Drice::V5::TurboID-2* (5′-TTCGGCGCCGGCCTGGCGCACAGG-3′ and 5′-AAACCCTGTGCGCCAGGCCGGCGC-3′), *Dronc::V5::TurboID-1* (5′-TTCGGCCAAGTCTTGCCGACACTC-3′ and 5′-AAACGAGTGTCGGCAAGACTTGGC-3′), *Dronc::V5::TurboID-2* (5′-TTCGGTGATGCCTGAGTATGTAAT-3′ and 5′- AAACATTACATACTCAGGCATCAC-3′).

For generation of the homology-directed repair template, DNA fragments of the 5′ homology arm with V5::TurboID were assembled into the BsaI site and the DNA fragment of the 3′ homology arm was assembled into the SapI site of pBac[3xP3-DsRed_polyA_Scarless_TK] (generated by T. Katsuyama, the full sequence is given below) using NEBuilder HiFi DNA Assembly (New England Biolabs). The PAM sequences of the gRNA-binding sites in the donor template were mutated to prevent Cas9-directed cleavage following homology-directed repair. The V5::TurboID fragment was amplified from V5-TurboID-NES_pCDNA3 (#107169, Addgene). The DNA fragments were amplified by PCR using the following primers: *dcp-1* 5′ homology arm-1 with mutated PAM (forward primer, 5′-TGAAGGTCTCCTTAACTGATCTTCAACCACGAATT-3′, and reverse primer, 5′-GCCGTGCTCGCCGTGCGAGAGTATG-3′), *dcp-1* 5′ homology arm-2 with mutated PAM and

N-terminus of *V5::TurboID* (forward primer, 5′-CTCGCACGGCGAGCACGGCTACCTG-3′, and reverse primer, 5′-GGGGATGGGCTTGCCGCCAGCCTTATTGCCGTTCG-3′), *V5::TurboID* (forward primer, 5′-GGCAAGCCCATCCCCAACCCCCTGCTGGGCCTGGA-3′, and reverse primer, 5′-TCATCACTGCAGCTTTTCGGCAGACCGCAGACTGA-3′), *dcp-1* 5′ homology arm-3 with C-terminus of *V5::TurboID* (forward primer, 5′-AAGCTGCAGTGATGAGAAGAGATCTCCCTTCGAAG-3′, and reverse primer, 5′-TCTTTCTAGGGTTAAATGCATTAATAGTTCCTTCG-3′), *dcp-1* 3′ homology arm-1 with mutated PAM (forward primer, 5′-TCTTTCTAGGGTTAAATATGATCTCGATTTGAATT-3′, and reverse primer, 5′-GTTTCCCGGCTCCAAACTGCCCCGCTTCCC-3′), *dcp-1* 3′ homology arm-2 with mutated PAM (forward primer, 5′-TTGGAGCCGGGAAACTTAGCCAAGACGCCT-3′, and reverse primer, 5′-GACGGCTCTTCATTACATATTAGTGTGACGTTGTA-3′), *drice* 5′ homology arm-1 with mutated PAM (forward primer, 5′-TGAAGGTCTCCTTAACAAGATTCCAGTGCACGCCG-3′, and reverse primer, 5′-CGGAGTGTCGGGGGTGCAGGACTCA-3′), *drice* 5′ homology arm-2 with mutated PAM and N-terminus of *V5::TurboID* (forward primer, 5′-CTGCACCCCCGACACTCCGGAGATG-3′, and reverse primer, 5′-GGGGATGGGCTTGCCAACCCGTCCGGCTGGTGCCA-3′), *V5::TurboID* (forward primer, 5′-GGCAAGCCCATCCCCAACCCCCTGCTGGGCCTGGA-3′, and reverse primer, 5′-TCATCACTGCAGCTTTTCGGCAGACCGCAGACTGA-3′), *drice* 5′ homology arm-3 with C-terminus of *V5::TurboID* (forward primer, 5′-AAGCTGCAGTGATGATGGCTAATGGTATGGATCAA-3′, and reverse primer, 5′-TCTTTCTAGGGTTAAATTTCTCTGAATTCAACCCA-3′), *drice* 3′ homology arm-1 with mutated PAM (forward primer, 5′-TCTTTCTAGGGTTAAAGCCTGTCAGCAAATCCGAC-3′, and reverse primer, 5′-GAGGATCGTCCTGTGCGCCAGGCCGGCGCC-3′), *drice* 3′ homology arm-2 with mutated PAM (forward primer, 5′-CACAGGACGATCCTCCACGGAGATGACCTCGATGC-3′, and reverse primer, 5′-GACGGCTCTTCATTACCGTCTCCGTGGGCCCGGCC-3′), *dronc* 5′ homology arm-1 with mutated PAM (forward primer, 5′-TGAAGGTCTCCTTAACAAATGTCCTTATTTGGTGA-3′, and reverse primer, 5′-ATAGCAGACGAGAGTGTCGGCAAGA-3′), *dronc* 5′ homology arm-2 with mutated PAM and N-terminus of *V5::TurboID* (forward primer, 5′-CGACACTCTCGTCTGCTATGCTAAT-3′, and reverse primer, 5′-GGGGATGGGCTTGCCTTCGTTGAAAAACCCGGGAT-3′), *V5::TurboID* (forward primer, 5′-GGCAAGCCCATCCCCAACCCCCTGCTGGGCCTGGA-3′, and reverse primer, 5′-TCATCACTGCAGCTTTTCGGCAGACCGCAGACTGA-3′), *dronc* 5′ homology arm-3 with C-terminus of *V5::TurboID* (forward primer, 5′-AAGCTGCAGTGATGATTGCCGCCACTGGACATTTT-3′, and reverse primer, 5′-TCTTTCTAGGGTTAATTATATACAAACTGCGGTTT-3′), *dronc* 3′ homology arm-1 with mutated PAM (forward primer, 5′-TCTTTCTAGGGTTAAAATCTATTTACATTTCTAAAATTTCATTGGGACAC-3′, and reverse primer, 5′-TGTAATTGCCCAAAAGCCGCATAAGCCAAA-3′), *dronc* 3′ homology arm-2 with mutated PAM (forward primer, 5′-TTTTGGGCAATTACATACTCAGGCATCACC-3′, and reverse primer, 5′-GACGGCTCTTCATTAGACAGGTGATGAACTACCGC-3′). The detailed plasmid DNA sequences are available upon request. The transgenic flies were generated by BestGene Inc. Each DsRed-positive transformant was isogenized and confirmed by genomic PCR and sequencing.

Gal4 expression check. Larvae and pupae were digitized using a fluorescent stereomicroscope Leica MZ16F (Leica Microsystems) equipped with a CCD camera. Imaginal discs of early (feeding) and late (wandering) 3rd instar larvae were dissected, followed by immunohistochemical staining (details are described below).

Wing size, cell size, cell number and leg length measurements. Flies were placed on acetic acid agar plate (2% agar, 1% sucrose, 0.36% acetic acid) to lay eggs overnight. The plates were collected and the eggs were incubated at 25 °C for 24 hours. The 1st instar larvae were collected form the agar plate and 30 larvae were placed in one vial for precisely controlling the larval density. These flies were raised at 25 °C. After more than 2 days of hatching, the adult female flies were collected and submerged into 99.5 % ethanol to dehydrate for 24 hours. The dehydrated flies were dissected to mount their wings and hind legs using Euparal (Waldeck) with the dorsal side upward. Images were digitized using an upright microscope Leica DM5000B (Leica Microsystems) equipped with a CCD camera. Wing sizes and leg lengths were measured using the ImageJ (NIH) software (see SI Appendix, Fig. S2A and C for more details). For cell size and cell number measurements, the proximal area of the rectangle (0.035 mm^2 except for *C10 > p35* (0.028 mm^2), th^4, *wp > InR*^{DN} (0.028 mm^2) and *wp > InR*^{DN} (0.022 mm^2)) between the L2 and L3 veins (see SI Appendix, Fig. S2B for more details) was analyzed by counting the small bristles on the dorsal side. The total cell number was calculated using cell density and wing area.

Pupal size measurement. Pupae were put on glass slide with double-sided tape with the dorsal aspect up. The pupae were digitized using a fluorescent stereomicroscope Leica MZ16F (Leica Microsystems) equipped with a CCD camera. The pupal case sizes were measured using ImageJ (see SI Appendix, Fig. S3A for more details). After taking pictures, the pupae were placed into a 96-well plate one by one. After hatching, the sex of each individual was scored, for which the female pupal case sizes were used.

Fluctuating asymmetry measurement. Both the right and left wings were mounted and measured as mentioned above. To minimize measurement error, each wing was measured twice ($R_{M1,i}$ and $R_{M2,i}$). The average wing size from the two measurements ($R_{ave,i} = (R_{M1,i} + R_{M2,i}) / 2$) was used for further analysis. For each fly, the difference of right - left wing size ($D_i = R_{ave,i} - L_{ave,i}$) was calculated. For each genotype, the average difference of right - left ($D_{ave} = \sum_{i=1}^{n} D_i$ / n) was subtracted from D_i to correct the directional asymmetry ($adjD_i = D_i - D_{ave}$). For statistical analysis, the absolute values of $adjD_i$ ($|adjD_i|$) of each group were subjected to Mann-Whitney *U* test.

Pupation time measurement. Flies were placed on acetic acid agar plate to lay eggs for 4 hours. The plates were collected (After Egg Laying (AEL) 0 h) and the eggs were incubated at 25 °C for an additional 24 hours. The 1st instar larvae were collected from the agar plate (After Egg Hatching (AEH) 0 h, which corresponds to AEL 24 h) and 30 larvae were placed into one vial for precisely controlling the larval density per vials. These flies were raised at 25 °C. The newly formed pupae were counted every 8 hours from AEH 136 h to AEH 216 h and AEH 288 h.

Curly-up and opaque (cell remaining) fly wing scoring and screening. Wing phenotypes were scored after more than 2 days of hatching. The RNAi screening was blinded. For image acquisition, adult female flies were anesthetized with CO_2. The top view images were digitized using a fluorescent stereomicroscope Leica MZ16F (Leica Microsystems) equipped with a CCD camera. The side view images were digitized using a α6500 camera (Sony) equipped with Makro-Planar 60 mm F2.8 lens (Carl Zeiss). For the remaining wing cell DNA staining, 4 mM Hoechst 33342 (#H3570, Invitrogen) was injected into the adult abdomen using FemtoJet 4i (Eppendorf). Glass capillaries were generated from Drummond Microcaps, 30 µl (Drummond Scientific Company), using PC-10 Puller (Narishige). One hour after the injection, the wings were removed and mounted using Euparal (Waldeck). Images were digitized using an upright microscope Leica DM4000B (Leica Microsystems) equipped with a CCD camera.

Immunohistochemistry. The WDs of late 3rd instar larvae were fixed with 4% paraformaldehyde (PFA) in PBS. The pupal wings of 24 h After Puparium Formation (APF) were dissected following

the protocol described previously (21) and fixed with 4% PFA in PBS. The samples were washed in PBS plus 0.1% Triton X-100 (PBST) and subsequently blocked in PBST with 5% normal donkey serum (PBSTn) for 30 min, and incubated with primary antibodies in PBSTn overnight at 4 °C. Next, the samples were washed with PBST and incubated for 2 h with secondary antibodies in PBSTn, and again washed with PBST. Images were taken with Leica TCS SP8 or Leica TCS SP5 confocal microscope (Leica Microsystems). The primary antibodies used included mouse anti-Nubbin antibody (1:10, gift from S. Cohen), rabbit anti-phospho Histone H3 (Ser10) antibody (1:100, #06-570, Millipore), rat anti-mCD8 antibody (1:500, #MCD0800, Invitrogen), rabbit anti-cPARP antibody (Y34) (1:250, #ab32561, Abcam), and mouse anti-V5 antibody (1:200, #R960-25, Invitrogen). The secondary antibodies used included Alexa Fluor 647-conjugated goat anti-mouse IgG (1:500, #A-21240, Molecular Probes), Alexa Fluor 488-conjugated goat anti-rat IgG (1:500, #A-11006, Molecular Probes), Alexa Fluor 568-conjugated donkey anti-rabbit IgG (1:500, #A-10042, Molecular Probes), and Cy3-conjugated donkey anti-mouse IgG (1:500, #715-165-151, Jackson Immuno Research). Streptavidin Alexa Fluor 633-conjugate (1:500, #S21375, Invitrogen) for biotinylated proteins staining and 4 μM Hoechst 33342 (#H3570, Invitrogen) for nuclear staining were used during the secondary antibody incubation. Images were analyzed and edited using ImageJ.

Quantification of WD volume. Images were taken at every 1 μm increment along the z-axis. Image stacks were used for volume quantification. The dorsal volume ratio was quantified by measuring the total Nubbin volume and GFP-positive Nubbin volume using ImageJ, following the calculation of the ratio of dorsal GFP-positive Nubbin volume against the total Nubbin volume. The images were analyzed semi-automatically using ImageJ macro. Briefly, the Nubbin channel was filtered by "Gaussian Blur 3D (x = 1, y = 1, z = 1)", and processed with "Make Binary" ("Otsu" method), and the Nubbin volume was measured by "Analyze particles". Next, the GFP channel was filtered by "Gaussian Blur 3D (x = 1, y = 1, z = 1)", and processed with "Make Binary" ("Otsu" method) to define the GFP-positive ROI. Applying the defined ROI to the Nubbin channel, which is primarily processed by "Gaussian Blur 3D (x = 1, y = 1, z = 1)" and processed with "Make Binary" ("Otsu" method), GFP-positive Nubbin volume was measured.

Terminal deoxynucleotidyl transferase dUTP nick end labeling (TUNEL) assay. TUNEL assay was performed using the ApopTag Red in situ apoptosis detection kit (Millipore) according to the manufacturer's instruction. The WDs were dissected and fixed for 20 min at room temperature in 1% PFA in PBS. The samples were then washed with PBS three times, 5 min per wash. Next, the samples were re-fixed in ethanol: acetic acid, 2:1, for 5 min at -20 °C; washed in PBS twice, 5 min per wash; incubated in equilibration buffer (ApopTag kit; Millipore) for 10 sec; and incubated again in reaction buffer (TdT enzyme; ratio 7:3; ApopTag kit) at 37 °C for 1 h. The TdT reaction mix was replaced with stop buffer (diluted 1:34 in dH_2O; ApopTag kit) and incubated for 10 min at room temperature. Then, the samples were washed three times with PBS, 1 min per wash; and incubated with anti-digoxigenin antibody solution (diluted 31:34 in blocking solution; ApopTag kit) for 30 min at room temperature. The samples were then washed four times in PBS, 2 min per wash. For the subsequent antibody staining, the samples were blocked in PBSTn for 30 min, and incubated with primary antibodies in PBSTn overnight at 4 °C. The samples were next washed with PBST and incubated for 2 h with secondary antibodies in PBSTn, and then again washed with PBST. The primary antibody used is rabbit anti-GFP antibody (1:500, #598, MBL). The secondary antibody used is Alexa Fluor 488-conjugated donkey anti-rabbit IgG (1:500, #A-21206, Molecular Probes).

Quantification of the TUNEL and cPARP ratio. Images were taken at every 4 μm increment along the z-axis. Maximum intensity projection images were used for quantification. The TUNEL/cPARP ratio was quantified by measuring the area of the TUNEL/cPARP-positive and

GFP/mCD8-positive pixels using ImageJ, by calculating the ratio of TUNEL/cPARP stained pixels to GFP/mCD8 stained pixels. The images were analyzed semi-automatically using ImageJ macro. Briefly, the GFP/mCD8 channel was processed by "Auto Threshold" ("Huang" method), and the GFP/mCD8-positive area was defined by "Analyze particles." Within the GFP/mCD8-positive area, the TUNEL/cPARP channel was processed by "Auto Threshold" ("MaxEntropy" method), and the TUNEL/cPARP-positive area was defined by "Analyze particles."

Western Blotting. For the experiments shown in Fig. 4B and SI Appendix, Fig. S9, the wandering 3rd instar larvae were irradiated with 50 mJ/cm^2 using FUNA UV Crosslinker FS-1500 (Funakoshi) and incubated at 25 °C for 8 hours. Three wandering 3rd instar larvae were dissected to remove the digestive tract and the fat body. The remnants were rinsed with PBS twice and then homogenized with 60 µl lysis buffer (1% NP40, 500 mM NaCl, 20 mM EDTA, 10 mM NaF, 1xcOmplete, EDTA-free Protease Inhibitor Cocktail (Roche), 1 mM PMSF, 2 mM Benzamidine, 500 mM Tris-HCl (pH 7.4)). The samples were centrifuged (15,000 g, 5 min, 4 °C) and 50 µl supernatant was collected and mixed with 10 µl 6x Laemmli sample buffer. For the experiment shown in Fig. 5J, 30 WDs of the late 3rd instar larvae were dissected and rinsed with PBS once and then homogenized with 45 µl 1x Laemmli sample buffer. The samples were boiled for 5 min at 95 °C and centrifuged (15,000 g, 5 min, 4 ℃). For the experiments shown in Fig. 4B and SI Appendix, Fig. S9, 20 µl (approximately 100 µg protein) of each sample was separated by 15% SDS-PAGE. For the experiment shown in Fig. 5J, the samples were separated by 12.5% SDS-PAGE. Then, the proteins were transferred to Immobilon-P PVDF membranes (Millipore) for immunoblotting. The membranes were blocked with 4% skimmed milk for 30 min. Immunoblotting was performed with the antibodies mentioned below that were diluted with Can Get signal immunoreaction enhancer (TOYOBO) solution 1 (for 1st antibodies) and solution 2 (for 2nd antibodies). Antibodies and their dilutions used are as follows: mouse anti-myc monoclonal antibody (1:10,000 for both full length SCAT3 and cleaved SCAT3 (SI Appendix, Fig. S9), 1:1,000 for cleaved SCAT3 (Fig. 4B), #R950-25, Invitrogen), mouse anti-V5 monoclonal antibody (1:5,000, #46-0705, Invitrogen), mouse anti-Histone H3 monoclonal antibody (1B1B2) as a loading control (1:10,000, #14269, Cell Signaling Technology), and anti-mouse IgG HRP Conjugate (1:10,000, #W402B, Promega). The membrane for streptavidin blotting was blocked with 3% BSA. Streptavidin blotting was performed with streptavidin-HRP (1:20,000, #SA10001, Invitrogen) diluted with Can Get signal immunoreaction enhancer solution 2. The signals were visualized using Immobilon Western Chemiluminescent HRP Substrate (Millipore) and FUSION SOLO. 7S. EDGE (Vilber-Lourmat). Contrast and brightness adjustment were applied equally using Evolution Capt software (Vilber-Lourmat).

Microarray sample preparation and analysis. For microarray analysis, 20 WDs of female wandering 3rd instar larvae were collected. Total RNA was extracted by QIAzol Lysis Reagent (QIAGEN), followed by purification using the RNeasy Plus Micro Kit (QIAGEN). We used 200 ng total RNA for the analysis using the Drosophila V2 microarray, according to the manufacturer's instructions (Agilent SureScan). Quintuplicate samples were used for each genotype. The data were analyzed using R software. Using the Linear Models for Microarray (limma) package (22, 23), the single-channel Agilent intensity data were read with modified *read.maimages*. Then, the data were normalized with *normalizeBetweenArrays (method = "quantile")*. Principal component analysis was performed by *prcomp.* Differential expression analysis was performed using linear models and empirical bayes methods (22). GO analysis was performed using DAVID (24, 25) with a statistical significance of $q < 0.05$ for up- or down-regulated genes. The microarray data are available at the NCBI Gene Expression Omnibus (https://www.ncbi.nlm.nih.gov/geo/) under series accession number GSE136170.

Statistical analysis. Statistical analysis was performed using GraphPad Prism 7. The statistical tests used are described in the figure legends. Statistical significance is shown as follows; n.s., $P > 0.05$; *$P < 0.05$; **$P < 0.01$; ***$P < 0.001$; ****$P < 0.0001$.

Detailed genotypes of the flies used in the figures.

Fig. 1B-D (Left to Right):
UAS-LacZ/+; *C10-Gal4/+* (w^{1118} genetic background)
C10-Gal4/UAS-Dronc^{DN} (w^{1118} genetic background)
UAS-p35/+; *C10-Gal4/+* (w^{1118} genetic background)

Fig. 1E and F (Left to Right):
UAS-p35/+ (w^{1118} genetic background)
UAS-p35/+; *C10-Gal4/+* (w^{1118} genetic background)

Fig. 1G-G'' (Left to Right):
UAS-GFP/+; *C10-Gal4/+* (w^{1118} genetic background)
C10-Gal4/UAS-Dronc^{DN} (w^{1118} genetic background)
UAS-p35/+; *C10-Gal4/+* (w^{1118} genetic background)

Fig. 2A-C (Left to Right):
WP-Gal4, UAS-mCD8::GFP/+
WP-Gal4, UAS-mCD8::GFP/th^{4}
WP-Gal4, UAS-InR^{DN}/+
WP-Gal4, UAS- InR^{DN}/th^{4}

Fig. 3A and B (Left to Right):
w^{1118}
C10-Gal4/+ (w^{1118} genetic background)
UAS-LacZ-RNAi/+
UAS-LacZ-RNAi/+; *C10-Gal4/+*
UAS-dark-RNAi (V100405)*/+*
UAS-dark-RNAi (V100405)*/+*; *C10-Gal4/+*
UAS-dronc-RNAi (V23035)*/+*
UAS-dronc-RNAi (V23035)*/+*; *C10-Gal4/+*
UAS-drice-RNAi (V28065)*/+*
UAS-drice-RNAi (V28065)*/+*; *C10-Gal4/+*
UAS-dcp-1-RNAi (V107560)*/+*
UAS-dcp-1-RNAi (V107560)*/+*; *C10-Gal4/+*
UAS-decay-RNAi (V43028)*/+*
UAS-decay-RNAi (V43028)*/+*; *C10-Gal4/+*
UAS-decay-RNAi (V100168)*/+*
UAS-decay-RNAi (V100168)*/+*; *C10-Gal4/+*

Fig. 4B (Left to Right):
w^{1118}
Act5C-Gal4, UAS-SCAT3^{DEVD}/+; *dronc$^{\Delta A8}$/+*
Act5C-Gal4, UAS-SCAT3^{DEVD}/+; *dronc$^{\Delta A8}$/dronc$^{\Delta A8}$*
Act5C-Gal4, UAS-SCAT3^{DEVD}/+; *dronc$^{\Delta A8}$/th^{4}*
Act5C-Gal4, UAS-SCAT3^{DEVD}/+; *dronc$^{\Delta A8}$/th^{4}, dronc$^{\Delta A8}$*
Act5C-Gal4, UAS-SCAT3^{DEVD}/+; *dronc$^{\Delta A8}$/+*
Act5C-Gal4, UAS-SCAT3^{DEVD}/+; *dronc$^{\Delta A8}$/dronc$^{\Delta A8}$*
Act5C-Gal4, UAS-SCAT3^{DEVD}/UAS-p35; *dronc$^{\Delta A8}$/+*
Act5C-Gal4/UAS-SCAT3^{DEVG}

Fig. 5D-D'': *dcp-1::V5::TurboID, apterous-Gal4, UAS-mCD8::GFP/UAS-LacZ-RNAi*

Fig. 5E-E'': *dcp-1::V5::TurboID, apterous-Gal4, UAS-mCD8::GFP/UAS-dcp-1-RNAi* (V107560)

Fig. 5F-F'': *apterous-Gal4, UAS-mCD8::GFP/UAS-LacZ-RNAi*; *drice::V5::TurboID/+*

Fig. 5G-G'': *apterous-Gal4, UAS-mCD8::GFP/UAS-drice-RNAi* (V28065); *drice::V5::TurboID/+*

Fig. 5H-H'': *apterous-Gal4, UAS-mCD8::GFP/UAS-LacZ-RNAi*; *dronc::V5::TurboID/+*

Fig. 5I-I'': *apterous-Gal4, UAS-mCD8::GFP/UAS-dronc-RNAi* (V23035); *drice::V5::TurboID/+*

Fig. 5J (Left to Right):
w^{1118}
dcp-1::V5::TurboID/+
drice::V5::TurboID/+
dronc::V5::TurboID/+

Fig. 6B (Left to Right):
acn^{27}*/Df(2R)ED1200*; *acnP-myc-*Acn^{WT}*/+*
acn^{27}*/Df(2R)ED1200*; *acnP-myc-*Acn^{D527A}*/+*
acn^{27}*/Df(2R)ED1200*; *acnP-myc-*Acn^{WT}*/*th^{4}
acn^{27}*/Df(2R)ED1200*; *acnP-myc-*Acn^{D527A}*/*th^{4}

SI Appendix, Fig. S1:
UAS-GFP/+ (Left in A, A', B, B' and C''')
C10-Gal4/UAS-GFP (Right in A, A', B, B' and C-C'')

SI Appendix, Fig. S2A and B: *UAS-LacZ/+*; *C10-Gal4/+* (w^{1118} genetic background)

SI Appendix, Fig. S2C: *UAS-GFP/+*; *C10-Gal4/+* (w^{1118} genetic background)

SI Appendix, Fig. S3A: *UAS-LacZ/+*; *C10-Gal4/+* (w^{1118} genetic background)

SI Appendix, Fig. S3B and C (Left to Right):
UAS-LacZ/+; *C10-Gal4/+* (w^{1118} genetic background)
UAS-p35/+; *C10-Gal4/+* (w^{1118} genetic background)

SI Appendix, Fig. S4A-C and D-D'' (Left to Right):
UAS-miRHG/+ (w^{1118} genetic background)
UAS-miRHG/+; *C10-Gal4/+* (w^{1118} genetic background)

SI Appendix, Fig. S5A-C (Left to Right):
apterous-Gal4, UAS-mCD8::GFP/+
apterous-Gal4, UAS-mCD8::GFP/UAS-p35

SI Appendix, Fig. S6A: *apterous-Gal4, UAS-mCD8::GFP/UAS-LacZ-RNAi*

SI Appendix, Fig. S6B: *apterous-Gal4, UAS-mCD8::GFP/UAS-p35*

SI Appendix, Fig. S6C: *apterous-Gal4, UAS-mCD8::GFP/UAS-miRHG*

SI Appendix, Fig. S6D: *apterous-Gal4, UAS-mCD8::GFP/+*; *UAS-Dronc^{DN}/+*

SI Appendix, Fig. S6E: *apterous-Gal4, UAS-mCD8::GFP/UAS-dark-RNAi* (V100405)

SI Appendix, Fig. S6G: *apterous-Gal4, UAS-mCD8::GFP/UAS-dronc-RNAi* (V23035)

SI Appendix, Fig. S6H: *apterous-Gal4, UAS-mCD8::GFP/UAS-drice-RNAi* (V28065)

SI Appendix, Fig. S6I: *apterous-Gal4, UAS-mCD8::GFP/UAS-dcp-1-RNAi* (V107560)

SI Appendix, Fig. S6J: *apterous-Gal4, UAS-mCD8::GFP/UAS-decay-RNAi* (V43028)

SI Appendix, Fig. S6K: *apterous-Gal4, UAS-mCD8::GFP/+*; *UAS-decay-RNAi* (V43029)*/+*

SI Appendix, Fig. S6L: *apterous-Gal4, UAS-mCD8::GFP/UAS-decay-RNAi* (V100168)

SI Appendix, Fig. S7A: *apterous-Gal4, UAS-mCD8::GFP/CyO* was crossed to each *UAS-RNAi* line.

SI Appendix, Fig. S7B: *apterous-Gal4, UAS-mCD8::GFP/CyO*; *UAS-Dcr2/TM6B* was crossed to each *UAS-RNAi* line.

SI Appendix, Fig. S8A and G: *UAS-LacZ-RNAi/+*; *C10-Gal4, UAS-GFP/+*

SI Appendix, Fig. S8B and G: *UAS-p35/+*; *C10-Gal4, UAS-GFP/+*

SI Appendix, Fig. S8C and G: *UAS-miRHG/+*; *C10-Gal4, UAS-GFP/+*

SI Appendix, Fig. S8D and G: *UAS-dcp-1-RNAi* (V107560)*/+*; *C10-Gal4, UAS-GFP/+*

SI Appendix, Fig. S8E and G: *UAS-decay-RNAi* (V43028)*/+*; *C10-Gal4, UAS-GFP/+*

SI Appendix, Fig. S8F and G: *UAS-decay-RNAi* (V100168)*/+*; *C10-Gal4, UAS-GFP/+*

SI Appendix, Fig. S8H and N: *UAS-LacZ-RNAi/+*; *C10-Gal4, UAS-mCD8::PARP::VENUS/+*

SI Appendix, Fig. S8I and N: *UAS-p35/+*; *C10-Gal4, UAS-mCD8::PARP::VENUS/+*

SI Appendix, Fig. S8J and N: *UAS-miRHG/+*; *C10-Gal4, UAS-mCD8::PARP::VENUS/+*

SI Appendix, Fig. S8K and N: *UAS-dcp-1-RNAi* (V107560)*/+*; *C10-Gal4, UAS-mCD8::PARP::VENUS/+*

SI Appendix, Fig. S8L and N: *UAS-decay-RNAi* (V43028)*/+*; *C10-Gal4, UAS-mCD8::PARP::VENUS/+*

SI Appendix, Fig. S8M and N: *UAS-decay-RNAi* (V100168)*/+*; *C10-Gal4, UAS-mCD8::PARP::VENUS/+*

SI Appendix, Fig. S9 (Left to Right):
w^{1118}
Act5C-Gal4, UAS-SCAT3^{DEVD}/+; *dronc*$^{\Delta A8}$/+
Act5C-Gal4, UAS-SCAT3^{DEVD}/+; *dronc*$^{\Delta A8}$/*dronc*$^{\Delta A8}$
Act5C-Gal4, UAS-SCAT3^{DEVD}/+; *dronc*$^{\Delta A8}$/*th*^{4}
Act5C-Gal4, UAS-SCAT3^{DEVD}/+; *dronc*$^{\Delta A8}$/*th*^{4}, *dronc*$^{\Delta A8}$
Act5C-Gal4, UAS-SCAT3^{DEVD}/+; *dronc*$^{\Delta A8}$/+
Act5C-Gal4, UAS-SCAT3^{DEVD}/+; *dronc*$^{\Delta A8}$/*dronc*$^{\Delta A8}$
Act5C-Gal4, UAS-SCAT3^{DEVD}/*UAS-p35*; *dronc*$^{\Delta A8}$/+
Act5C-Gal4/UAS-SCAT3^{DEVG}

SI Appendix, Fig. S10A and E: *w*^{1118}

SI Appendix, Fig. S10B and F: *dcp-1::V5::TurboID/*+

SI Appendix, Fig. S10C and G: *drice::V5::TurboID/*+

SI Appendix, Fig. S10D and H: *dronc::V5::TurboID/*+

SI Appendix, Fig. S11:
UAS-LacZ/+; *C10-Gal4/*+ (*w*^{1118} genetic background)
UAS-GFP/+; *C10-Gal4/*+ (*w*^{1118} genetic background)
UAS-p35/+; *C10-Gal4/*+ (*w*^{1118} genetic background)

SI Appendix, Fig. S12A: *apterous-Gal4, UAS-mCD8::GFP/*+

SI Appendix, Fig. S12B: *apterous-Gal4, UAS-mCD8::GFP/*+; *UAS-atg18a-RNAi* (BL28061)*/*+

SI Appendix, Fig. S12C: *apterous-Gal4, UAS-mCD8::GFP, UAS-dcp-1-RNAi* (V107560)*/*+

SI Appendix, Fig. S12D: *apterous-Gal4, UAS-mCD8::GFP, UAS-dcp-1-RNAi* (V107560)*/*+; *UAS-atg18a-RNAi* (BL28061)*/*+

SI Appendix, Fig. S12E (Left to Right):
apterous-Gal4, UAS-mCD8::GFP/CyO was crossed to each *UAS-RNAi* line.
apterous-Gal4, UAS-mCD8::GFP, UAS-dcp-1-RNAi (V107560)*/CyO* was crossed to each *UAS-RNAi* line.
apterous-Gal4, UAS-mCD8::GFP, UAS-decay-RNAi (V100168)*/CyO* was crossed to each *UAS-RNAi* line.

Sequence of pBac[3xP3-DsRed_polyA_Scarless_TK]

GGTCTCCTTAACCCTAGAAAGATAGTCTGCGTAAAATTGACGCATGCATTCTTGAAA
TATTGCTCTCTCTTTCTAAATAGCGCGAATCCGTCGCTGTGCATTTAGGACATCTCAG
TCGCCGCTTGGAGCTCCCGTGAGGCGTGCTTGTCAATGAGGTAAGTGTCACTGATTTT
GAACTATAACGACCGCGTGAGTCAAAATGACGCATGATTATCTTTTACGTGACTTTT
AAGATTTAACTCATACGATAATTATATTGTTATTTCATGTTCTACTTACGTGATAACTT
ATTATATATATATTTTCTTGTTATAGATATCCAATTCGGGATCTAATTCAATTAGAGA
CTAATTCAATTAGAGCTAATTCAATTAGGATCCAAGCTTATCGATTTCGAACCCTCGA
CCGCCGGAGTATAAATAGAGGCGCTTCGTCTACGGAGCGACAATTCAATTCAAACAA
GCAAAGTGAACACGTCGCTAAGCGAAAGCTAAGCAAATAAACAAGCGCAGCTGAAC
AAGCTAAACAATCGGCTCGAAGCCGGTCGCCACCATGGCCTCCTCCGAGGACGTCAT
CAAGGAGTTCATGCGCTTCAAGGTGCGCATGGAGGGCTCCGTGAACGGCCACGAGTT
CGAGATCGAGGGCGAGGGCGAGGGCCGCCCCTACGAGGGCACCCAGACCGCCAAGC
TGAAGGTGACCAAGGGCGGCCCCCTGCCCTTCGCCTGGGACATCCTGTCCCCCCAGT
TCCAGTACGGCTCCAAGGTGTACGTGAAGCACCCCGCCGACATCCCCGACTACAAGA
AGCTGTCCTTCCCCGAGGGCTTCAAGTGGGAGCGCGTGATGAACTTCGAGGACGGCG
GCGTGGTGACCGTGACCCAGGACTCCTCCCTCCAGGACGGCTCCTTCATCTACAAGG
TGAAGTTCATCGGCGTGAACTTCCCCTCCGACGGCCCCGTAATGCAGAAGAAGACTA
TGGGCTGGGAGGCGTCCACCGAGCGCCTGTACCCCCGCGACGGCGTGCTGAAGGGC
GAGATCCACAAGGCCCTGAAGCTGAAGGACGGCGGCCACTACCTGGTGGAGTTCAA
GTCCATCTACATGGCCAAGAAGCCCGTGCAGCTGCCCGGCTACTACTACGTGGACTC
CAAGCTGGACATCACCTCCCACAACGAGGACTACACCATCGTGGAGCAGTACGAGC
GCGCCGAGGGCCGCCACCACCTGTTCCTGTAGGGGCCGCGACTCTAGATCATAATCA
GCCATACCACATTTGTAGAGGTTTTACTTGCTTTAAAAAACCTCCCACACCTCCCCCT
GAACCTGAAACATAAAATGAATGCAATTGTTGTTGTTAACTTGTTTATTGCAGCTTAT
AATGGTTACAAATAAAGCAATAGCATCACAAATTTCACAAATAAAGCATTTTTTTCA
CTGCATTCTAGTTGTGGTTTGTCCAAACTCATCAATGTATCTTATTTGTTACTTTATAG
AAGAAATTTTGAGTTTTTGTTTTTTTTTAATAAATAAATAAACATAAATAAATTGTTT
GTTGAATTTATTATTAGTATGTAAGTGTAAATATAATAAAACTTAATATCTATTCAAA
TTAATAAATAAACCTCGATATACAGACCGATAAAACACATGCGTCAATTTTACGCAT
GATTATCTTTAACGTACGTCACAATATGATTATCTTTCTAGGGTTAATGAAGAGCCGT
CAATCGAGTTCAAGGGCGACACAAAATTTATTCTAAATGCATAATAAATACTGATAA
CATCTTATAGTTTGTATTATATTTTGTATTATCGTTGACATGTATAATTTTGATATCAA
AAACTGATTTTCCCTTTATTATTTTCGAGATTTATTTTCTTAATTCTCTTTAACAAACT
AGAAATATTGTATATACAAAAAATCATAAATAATAGATGAATAGTTTAATTATAGGT
GTTCATCAATCGAAAAAGCAACGTATCTTATTTAAAGTGCGTTGCTTTTTTCTCATTT
ATAAGGTTAAATAATTCTCATATATCAAGCAAAGTGACAGGCGCCCTTAAATATTCT
GACAAATGCTCTTTCCCTAAACTCCCCCCATAAAAAAACCCGCCGAAGCGGGTTTTT
ACGTTATTTGCGGATTAACGATTACTCGTTATCAGAACCGCCCAGGGGGCCCGAGCT
TAAGACTGGCCGTCGTTTTACAACACAGAAAGAGTTTGTAGAAACGCAAAAAGGCC
ATCCGTCAGGGGCCTTCTGCTTAGTTTGATGCCTGGCAGTTCCCTACTCTCGCCTTCC
GCTTCCTCGCTCACTGACTCGCTGCGCTCGGTCGTTCGGCTGCGGCGAGCGGTATCAG
CTCACTCAAAGGCGGTAATACGGTTATCCACAGAATCAGGGGATAACGCAGGAAAG
AACATGTGAGCAAAAGGCCAGCAAAAGGCCAGGAACCGTAAAAAGGCCGCGTTGCT
GGCGTTTTTCCATAGGCTCCGCCCCCCTGACGAGCATCACAAAAATCGACGCTCAAG
TCAGAGGTGGCGAAACCCGACAGGACTATAAAGATACCAGGCGTTTCCCCCTGGAA
GCTCCCTCGTGCGCTCTCCTGTTCCGACCCTGCCGCTTACCGGATACCTGTCCGCCTT
TCTCCCTTCGGGAAGCGTGGCGCTTTCTCATAGCTCACGCTGTAGGTATCTCAGTTCG
GTGTAGGTCGTTCGCTCCAAGCTGGGCTGTGTGCACGAACCCCCCGTTCAGCCCGAC
CGCTGCGCCTTATCCGGTAACTATCGTCTTGAGTCCAACCCGGTAAGACACGACTTAT

CGCCACTGGCAGCAGCCACTGGTAACAGGATTAGCAGAGCGAGGTATGTAGGCGGT
GCTACAGAGTTCTTGAAGTGGTGGGCTAACTACGGCTACACTAGAAGAACAGTATTT
GGTATCTGCGCTCTGCTGAAGCCAGTTACCTTCGGAAAAAGAGTTGGTAGCTCTTGA
TCCGGCAAACAAACCACCGCTGGTAGCGGTGGTTTTTTTGTTTGCAAGCAGCAGATT
ACGCGCAGAAAAAAAGGATCTCAAGAAGATCCTTTGATCTTTTCTACGGGGTCTGAC
GCTCAGTGGAACGACGCGCGCGTAACTCACGTTAAGGGATTTTGGTCATGAGCTTGC
GCCGTCCCGTCAAGTCAGCGTAATGCTCTGCTTTTACCAATGCTTAATCAGTGAGGCA
CCTATCTCAGCGATCTGTCTATTTCGTTCATCCATAGTTGCCTGACTCCCCGTCGTGTA
GATAACTACGATACGGGAGGGCTTACCATCTGGCCCCAGCGCTGCGATGATACCGCG
AGAACCACGCTCACCGGCTCCGGATTTATCAGCAATAAACCAGCCAGCCGGAAGGG
CCGAGCGCAGAAGTGGTCCTGCAACTTTATCCGCCTCCATCCAGTCTATTAATTGTTG
CCGGGAAGCTAGAGTAAGTAGTTCGCCAGTTAATAGTTTGCGCAACGTTGTTGCCAT
CGCTACAGGCATCGTGGTGTCACGCTCGTCGTTTGGTATGGCTTCATTCAGCTCCGGT
TCCCAACGATCAAGGCGAGTTACATGATCCCCCATGTTGTGCAAAAAAGCGGTTAGC
TCCTTCGGTCCTCCGATCGTTGTCAGAAGTAAGTTGGCCGCAGTGTTATCACTCATGG
TTATGGCAGCACTGCATAATTCTCTTACTGTCATGCCATCCGTAAGATGCTTTTCTGT
GACTGGTGAGTACTCAACCAAGTCATTCTGAGAATAGTGTATGCGGCGACCGAGTTG
CTCTTGCCCGGCGTCAATACGGGATAATACCGCGCCACATAGCAGAACTTTAAAAGT
GCTCATCATTGGAAAACGTTCTTCGGGGCGAAAACTCTCAAGGATCTTACCGCTGTT
GAGATCCAGTTCGATGTAACCCACTCGTGCACCCAACTGATCTTCAGCATCTTTTACT
TTCACCAGCGTTTCTGGGTGAGCAAAAACAGGAAGGCAAAATGCCGCAAAAAAGGG
AATAAGGGCGACACGGAAATGTTGAATACTCATATTCTTCCTTTTTCAATATTATTGA
AGCATTTATCAGGGTTATTGTCTCATGAGCGGATACATATTTGAATGTATTTAGAAAA
ATAAACAAATAGGGGTCAGTGTTACAACCAATTAACCAATTCTGAACATTATCGCGA
GCCCATTTATACCTGAATATGGCTCATAACACCCCTTGTTTGCCTGGCGGCAGTAGCG
CGGTGGTCCCACCTGACCCCATGCCGAACTCAGAAGTGAAACGCCGTAGCGCCGATG
GTAGTGTGGGGACTCCCCATGCGAGAGTAGGGAACTGCCAGGCATCAAATAAAACG
AAAGGCTCAGTCGAAAGACTGGGCCTTTCGCCCGGGCTAATTATGGGGTGTCGCCCT
TCGCTGAA

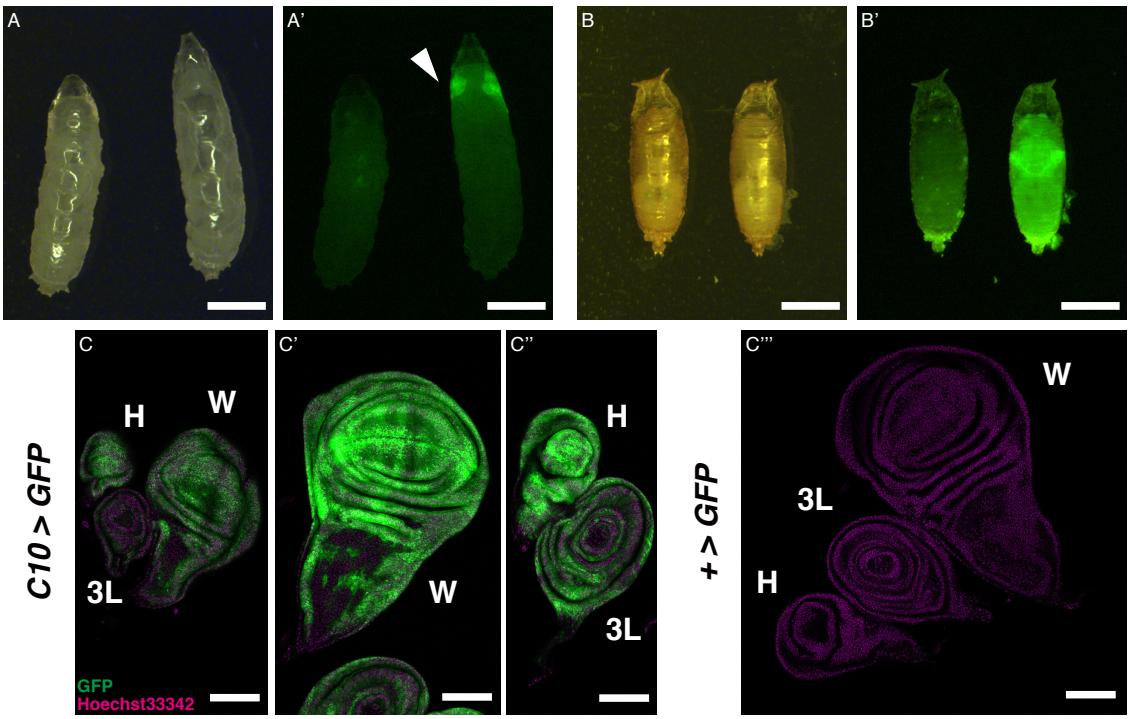

Fig. S1 Expression pattern of *C10-Gal4*. (A-B) Expression pattern of *C10-Gal4* in larva (A, A') and pupa (B, B'). The arrowhead indicates the position of WD. Genotypes: *+/UAS-GFP* (left), *C10-Gal4/UAS-GFP* (right). Scale bar: 1 mm. (C) Expression pattern of *C10-Gal4* in wing (W), haltere (H) and 3rd leg (3L) imaginal discs in early 3rd (C) and late 3rd (C', C'') larval stages compared with control (C'''). Genotypes: *C10-Gal4/UAS-GFP* (C-C''), *+/UAS-GFP* (C'''). Scale bar: 100 µm.

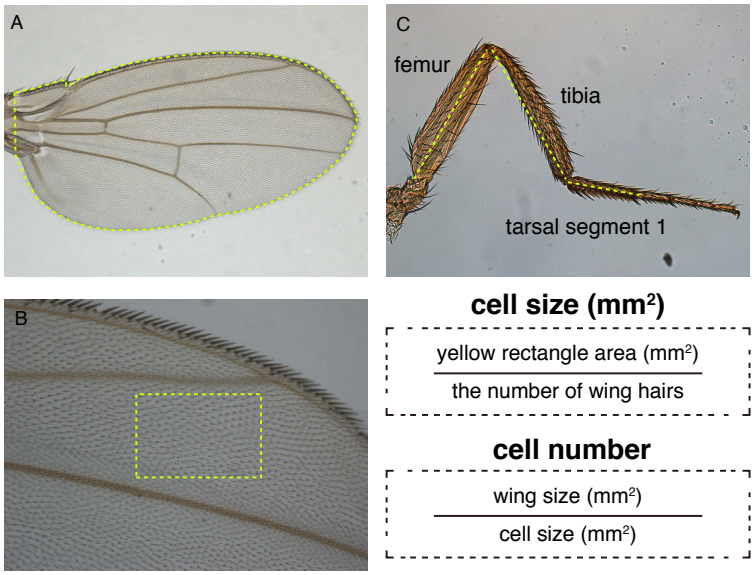

Fig. S2. Measurement parameters of *Drosophila* wings and legs. (A) Representative image of a *Drosophila* wing and yellow encircled region was measured to obtain the wing size. (B) Representative image of *Drosophila* wing hair. Hair number on the dorsal side of the yellow encircled region was counted for cell density measurement. (C) Representative image of a *Drosophila* hind leg. Yellow dotted lines were measured to obtain femur, tibia, and tarsal segment 1 lengths, respectively.

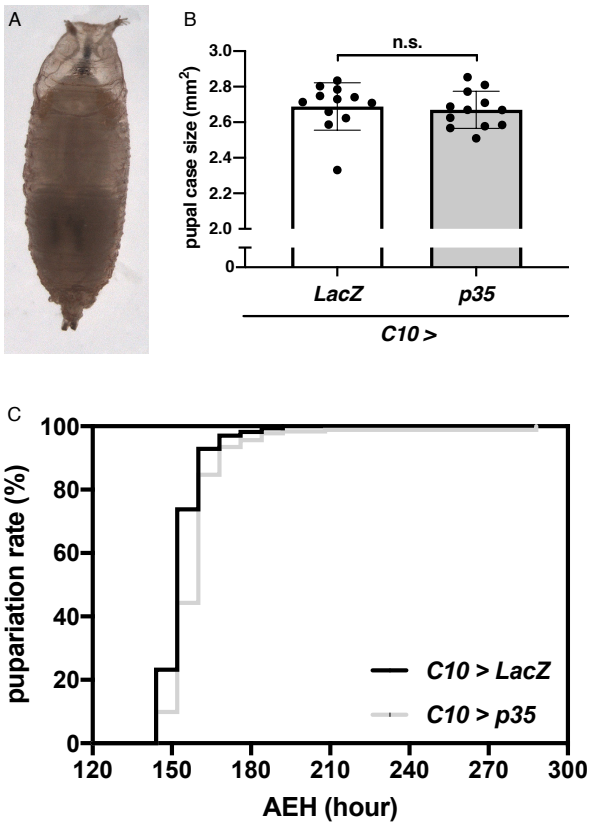

Fig. S3. Caspase inhibition affects neither overall body size nor larval developmental duration. (A) Representative image of a *Drosophila* pupa (used as an indicator of an overall body size (26)). (B) Pupal case sizes in control (*C10* > *LacZ*, n = 12) and caspase-inhibited flies (*C10* > *p35*, n = 12). Mean ± SD are shown. Statistical analysis was performed with unpaired Student's t-test. n.s., $P > 0.05$. (C) Pupation time (known to be linked with wing size (27)) for control (*C10* > *LacZ*, n = 168) and caspase-inhibited flies (*C10* > *p35*, n = 183). AEH, After Egg Hatching.

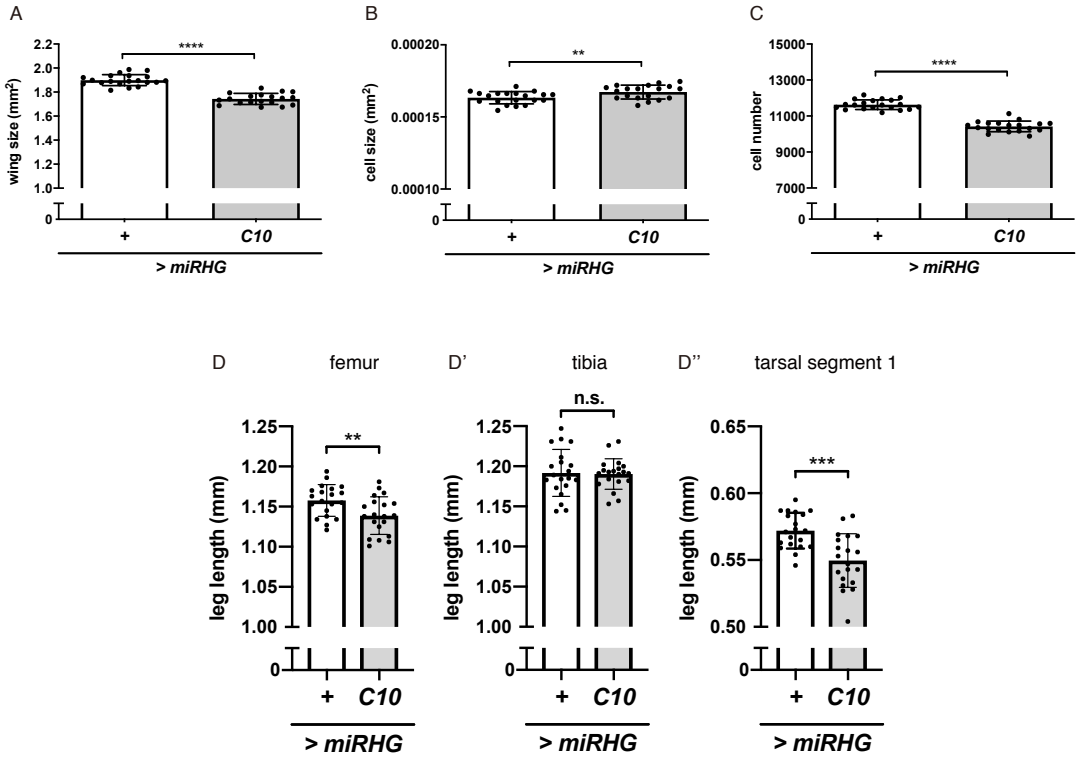

Fig. S4. Knockdown of *RHG* genes reduces imaginal tissue size. (A) Wing sizes in control (+ > *miRHG*, n = 20) and caspase-inhibited flies (*C10* > *miRHG*, n = 20). (B) Cell sizes and (C) cell numbers of (A). (D) Femur, (D') tibia, and (D'') tarsal segment 1 lengths in control (+ > *miRHG*, n = 20) and caspase-inhibited flies (*C10* > *miRHG*, n = 20). For all graphs, mean ± SD are shown. Statistical analyses were performed with unpaired Student's t-test. n.s., $P > 0.05$; **$P < 0.01$; ***$P < 0.001$; ****$P < 0.0001$.

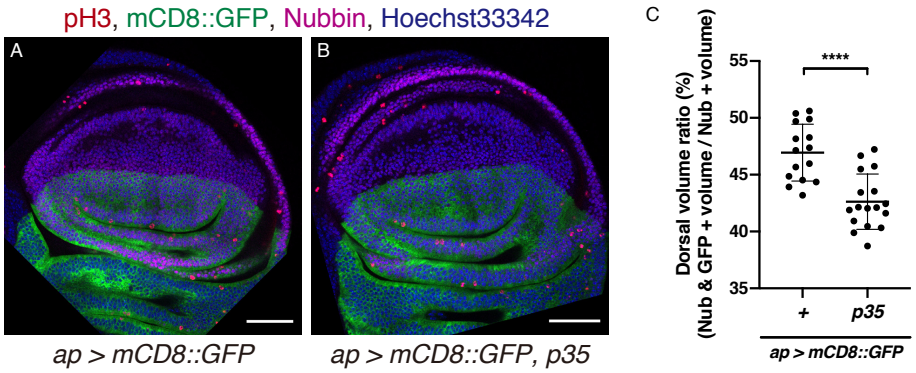

Fig. S5. Overexpression of *p35* reduces the volume of WD. (A, B) Representative images of WDs. pH3 (Red), mCD8::GFP (Green), Nubbin (Magenta), and Hoechst33342 (Blue). Scale bar: 50 μm. Sample sizes: *ap > mCD8::GFP*, n = 15 (A); *ap > mCD8::GFP, p35*, n = 17 (B). (C) Quantification of the ratio of dorsal wing pouch volume in (A) and (B). Mean ± SD are shown. Statistical analysis was performed with unpaired Student's t-test. ****$P < 0.0001$.

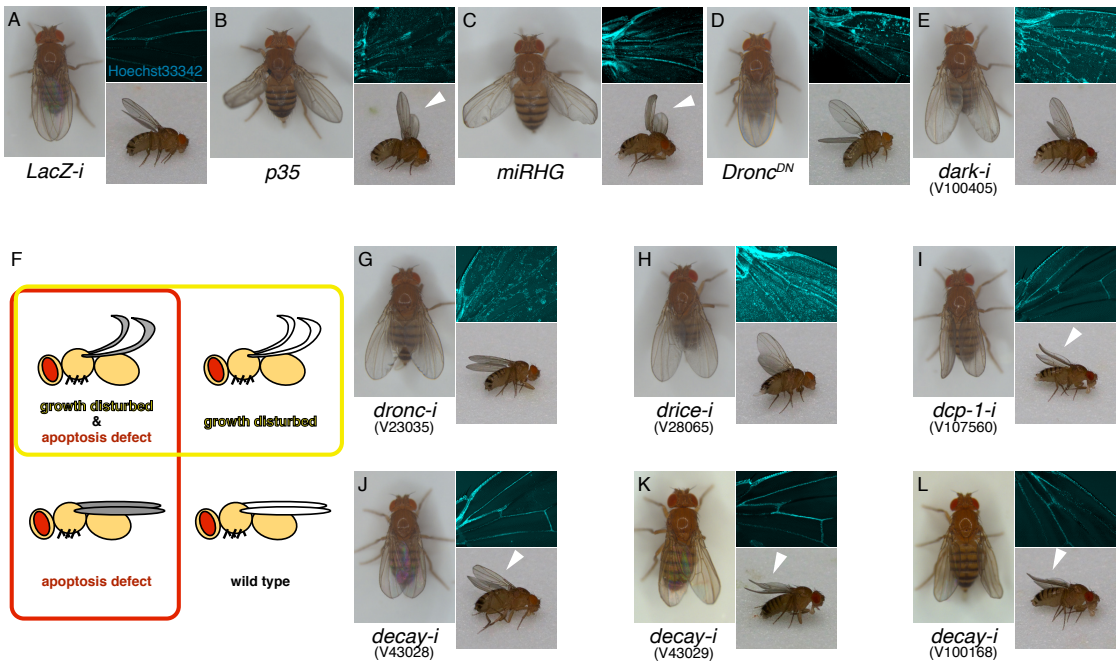

Fig. S6. The results of RNAi screening against *Drosophila* caspases. The wing is composed of two (dorsal/ventral) layers, and inhibiting the growth of the dorsal layer by *ap-Gal4* leads to the curly-up wing phenotype (14). Compared with the control of *LacZ* RNAi (A), *p35* overexpression (B) and *RHG* RNAi (C) showed curly-up wing, further supporting the idea that curly-up wing phenotype is derived from growth defects. In this screening, we also recorded the opaque wing phenotype which corresponds to defect in apoptosis (28). Indeed, *Dronc*^{DN} overexpression (D), *dark* RNAi (E) as well as *p35* overexpression (B) and *RHG* RNAi (C) flies showed opaque wing phenotype. We confirmed the remaining cells in opaque wing by staining the DNA (A-E). Thus, we determined whether RNAi suppressed wing growth and wing cell apoptosis by observing the adult wing phenotype (F). RNAi screening against all seven caspases revealed the opaque wing phenotypes without the curly-up wing phenotypes in all four *dronc* RNAi lines and two of the three *drice* RNAi lines (G, H, and SI Appendix, Fig. S7A), indicating that apoptosis was inhibited under these conditions. On the other hand, one out of five *dcp-1* RNAi line and three out of four *decay* RNAi lines showed the curly-up wing phenotypes without the opaque wing phenotypes or remaining wing cells (I-L and SI Appendix, Fig. S7A). By introducing *UAS-Dcr2* to enhance the RNAi efficiency, we also found the curly-up wing phenotypes in two *dcp-1* RNAi lines, two *strica* RNAi lines, and one *dredd* RNAi line (SI Appendix, Fig. S7B). In addition, one *drice* RNAi line showed the curly-up with opaque wing phenotype (SI Appendix, Fig. S7B). However, none of the *dronc* RNAi lines showed the curly-up wing phenotypes even in the presence of *UAS-Dcr2* (SI Appendix, Fig. S7B), suggesting the Dronc-independent nature of the wing growth promoting effect. (A-E) Representative images of adult female flies following inhibition of cell death signaling. Left panel, top view; bottom right panel, side view; arrowheads, curly-up wing; top right panel, DNA staining of fly wings 1 day after eclosion. *ap > mCD8::GFP, LacZ-i* (A), *ap > mCD8::GFP, p35* (B), *ap > mCD8::GFP, miRHG* (C), *ap > mCD8::GFP, Dronc*^{DN} (D), *ap > mCD8::GFP, dark-i*^{V100405} (E). (F) Schematic diagram of phenotypic-based screening for wing growth promoting caspases (G-L) Representative images of adult female flies for caspase RNAi screening with *ap > mCD8::GFP*. Left panel, top view; bottom right panel, side view; arrowheads, curly-up wing; top right panel, DNA staining of fly wings 1 day after eclosion. *ap > mCD8::GFP, dronc-i*^{V23035} (G), *ap > mCD8::GFP, drice-i*^{V28065} (H), *ap > mCD8::GFP, dcp-1-i*^{V107560} (I), *ap > mCD8::GFP, decay-i*^{V43028} (J), *ap > mCD8::GFP, decay-i*^{V43029} (K), *ap > mCD8::GFP, decay-i*^{V100168} (L).

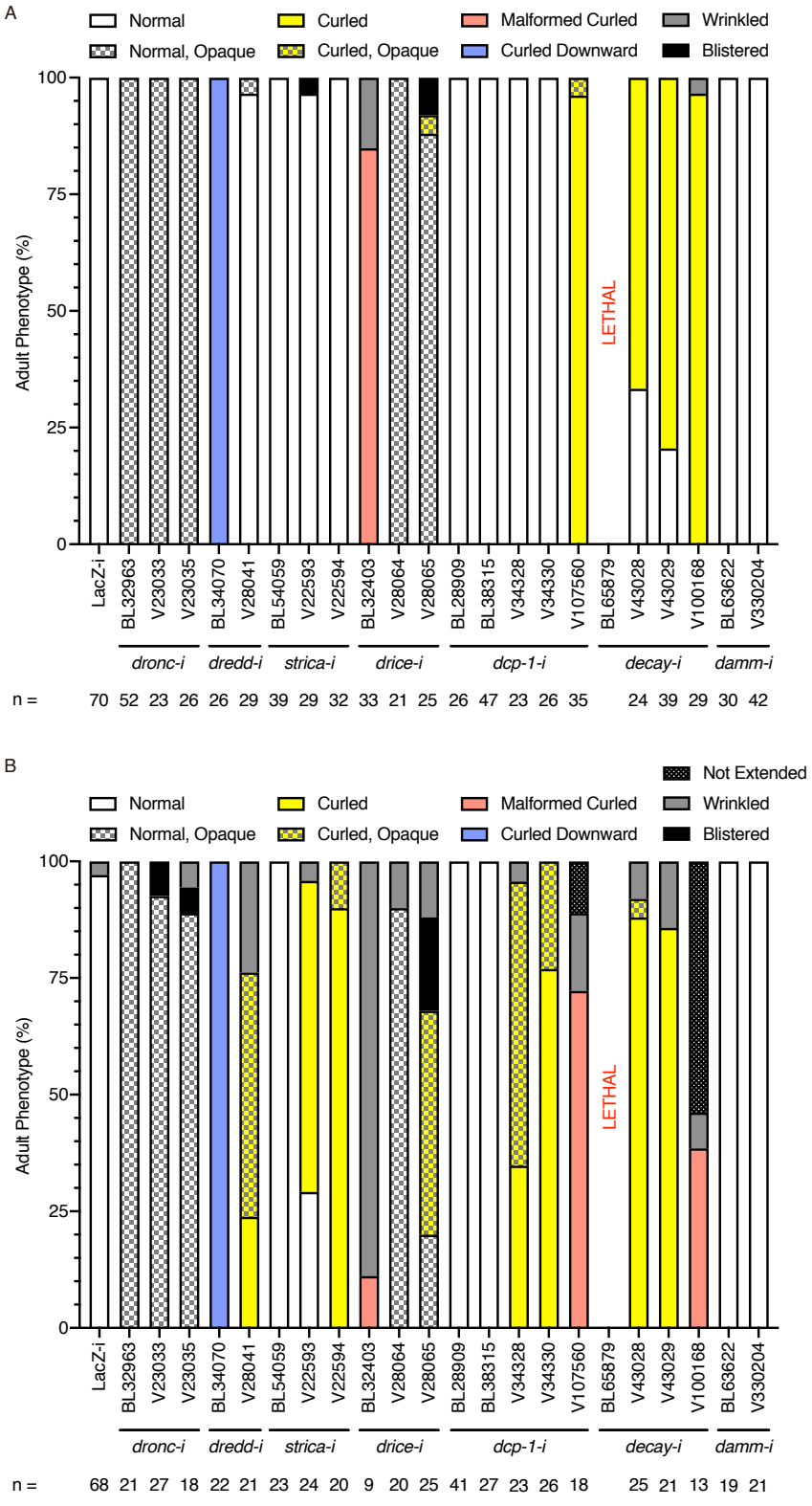

Fig. S7. The results of RNAi screening against *Drosophila* caspases. (A, B) RNAi screening results with *ap > mCD8::GFP* (A) and *ap > mCD8::GFP, Dcr2* (B) presented in 100% stacked column chart. Graph legends, genotypes, and sample sizes are included in the figures.

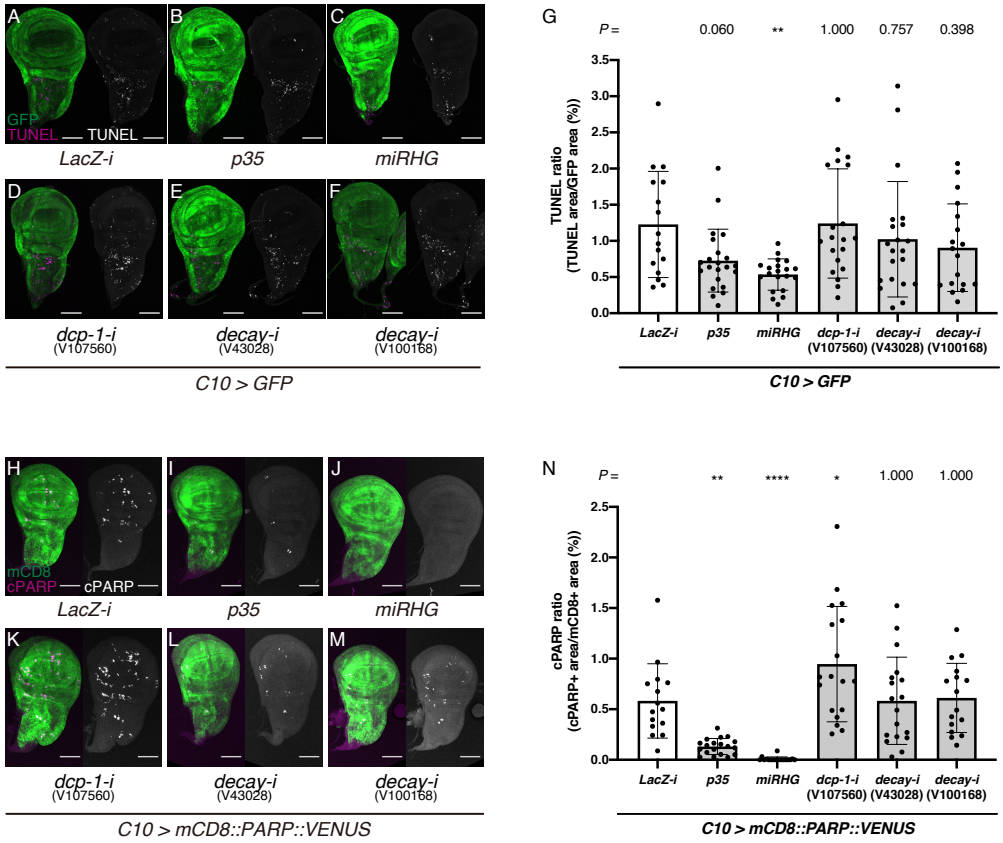

Fig. S8. The apoptosis rate is not correlated with wing size reduction. (A-F) Representative images of WDs observed using TUNEL assay. Left panel, merged image for GFP (Green) and TUNEL (Magenta) staining; right panel, TUNEL (Grey). Scale bar: 100 µm. Sample sizes: *C10 > GFP, LacZ-i*, n = 16 (A); *C10 > GFP, p35*, n = 22 (B); *C10 > GFP, miRHG*, n = 20 (C), *C10 > GFP, dcp-1-i*^{V107560}, n = 20 (D); *C10 > GFP, decay-RNAi*^{V43028}, n = 21 (E); *C10 > GFP, decay-i*^{V100168}, n = 18 (F). (G) Quantification of TUNEL ratio as the TUNEL-positive area per GFP-positive area. (H-M) Representative images of WDs expressing the mCD8::PARP::VENUS (CPV) probe. Left panel, merged mCD8 (Green) and cleaved PARP (cPARP, Magenta) staining; right panel, cPARP (Grey). Scale bar: 100 µm. Sample sizes: *C10 > CPV, LacZ-i*, n = 15 (H); *C10 > CPV, p35*, n = 19 (I); *C10 > CPV, miRHG*, n = 18 (J); *C10 > CPV, dcp-1-i*^{V107560}, n = 18 (K); *C10 > CPV, decay-i*^{V43028}, n = 18 (L); *C10 > CPV, decay-i*^{V100168}, n = 16 (M). (N) Quantification of cPARP ratio as the cPARP area per mCD8 area. Mean ± SD are shown. For all graphs, mean ± SD are shown. Statistical analysis was performed with Dunnett's multiple comparison test against control (*C10 > GFP, LacZ-i* (G) and *C10 > CPV, LacZ-i* (N)) after 1-way ANOVA. *$P < 0.05$; **$P < 0.01$; ****$P < 0.0001$.

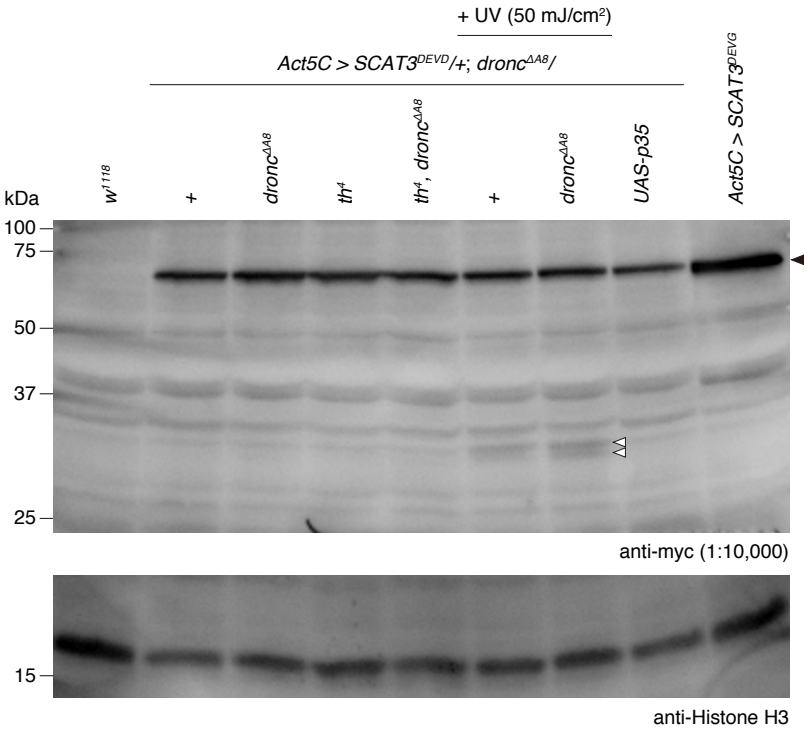

Fig. S9. Western blotting against full-length/cleaved SCAT3 probe (anti-myc antibody dilution 1:10,000) in the absence of Dronc. Genotypes are described in the figure. Black arrowhead, full-length SCAT3; white arrowheads, cleaved SCAT3.

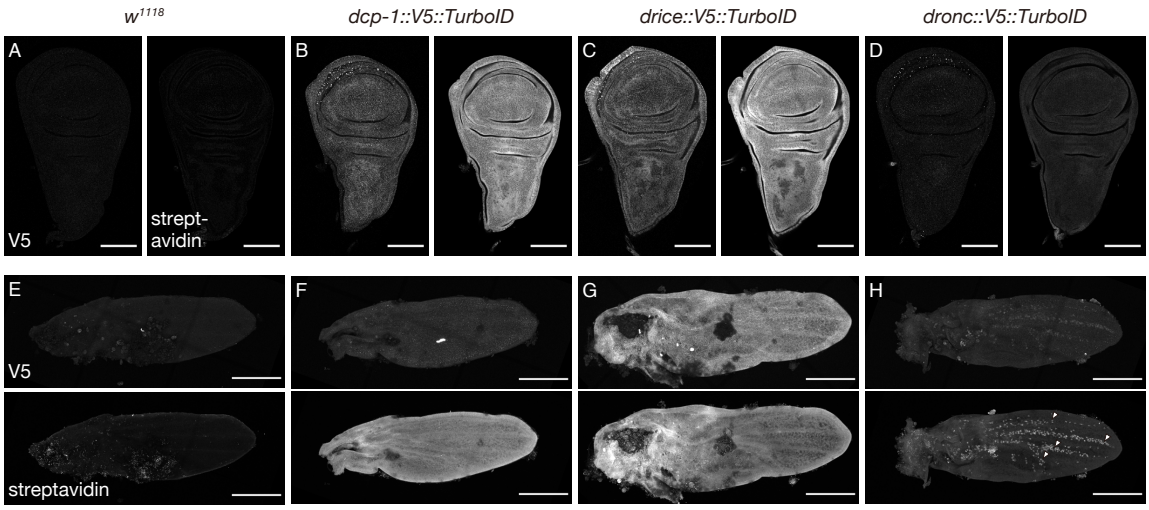

Fig. S10. Expression patterns of Dcp-1, Drice, and Dronc during wing development. (A-D) Expression patterns of Dcp-1 (B), Drice (C), and Dronc (D) in WDs compared with control (A). Left panel, V5 (Grey); right panel, streptavidin (Grey). Scale bar: 100 μm. Genotypes: w^{1118} (A), *dcp-1::V5::TurboID* (B), *drice::V5::TurboID* (C), *dronc::V5::TurboID* (D). (E-H) Expression patterns of Dcp-1 (F), Drice (G), and Dronc (H) in pupal wings at 24 h APF compared with control (E). Dcp-1 and Drice were expressed in wing epidermal cells and Dronc was highly expressed in hemocytes (white arrowheads). Top panel, V5 (Grey); bottom panel, streptavidin (Grey). Scale bar: 200 μm. Genotypes: w^{1118} (E), *dcp-1::V5::TurboID* (F), *drice::V5::TurboID* (G), *dronc::V5::TurboID* (H).

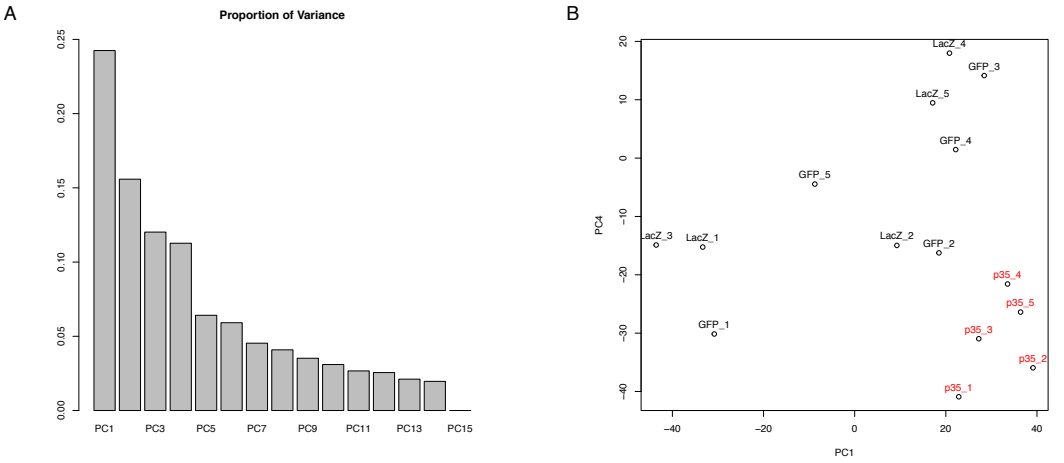

C

up regulated genes			down regulated genes		
GeneSymbol	logFC	q value	GeneSymbol	logFC	q value
msn	4.499589903	2.02E-09	CG31262	-3.533705394	2.69E-07
Cpr66D	1.804355542	9.29E-09	CG2277	-0.794930297	1.37E-06
CG5704	1.520471402	2.34E-08	CG42749	-0.943792973	4.55E-06
CG15211	2.053748291	2.69E-07	CG3857	-0.643608637	1.37E-05
pncr002:3R	1.019338302	8.39E-07	dpr17	-2.753236705	1.37E-05
CG33181	0.987810283	1.01E-06	Lip1	-2.406572063	2.23E-05
skd	1.19809536	1.93E-06	dob	-0.91247298	2.25E-05
CG33181	1.11175818	1.30E-05	CG9004	-0.453117688	4.85E-05
lara	0.684313109	1.30E-05	CG10089	-1.723323163	5.32E-05
CG1275	0.990695755	1.37E-05	CG7173	-1.241380086	0.000114134
CG9522	2.392749414	1.37E-05	CG11843	-0.718224801	0.000152595
CG5282	3.5859979	1.66E-05	CG42564	-1.276973683	0.000158355
CG15211	2.178204283	2.10E-05	CG32773	-0.951964462	0.00018621
CG5928	1.544643281	2.10E-05	dlg1	-0.481196044	0.000232024
m	0.706958955	5.17E-05	Ptr	-0.712529777	0.000232024
CG9521	1.568862637	5.32E-05	snoRNA:Psi28S-2566	-0.447765714	0.000255182
Calx37	0.483873458	6.03E-05	snoRNA:Psi28S-2566	-0.438351179	0.000307909
strica	0.826024795	6.29E-05	unc-13	-0.615161824	0.000316405
strica	0.825254055	6.88E-05	Filt	-1.201679264	0.000356704
CG18507	0.777599951	7.01E-05	CG32772	-0.464510453	0.000425678
sls	0.952645597	7.73E-05	CG11594	-1.301147593	0.000487088
CG33181	1.026871434	0.000152595	CG32055	-1.037730373	0.000529179
Cpr57A	1.081876949	0.00016388	CG12688	-0.550754487	0.000533772
CG14257	0.865860975	0.00018621	ppk	-0.949716473	0.000574703
CG5756	1.225954332	0.000232024	Ptr	-0.757752123	0.000598415

D

up-regulated genes (q<0.05)				
Term	Count	%	PValue	Benjamini
GO:0005975~carbohydrate metabolic process	7	3.684210526	0.001915597	0.631039591
GO:0006030~chitin metabolic process	6	3.157894737	0.007374563	0.854050031
GO:0045455~ecdysteroid metabolic process	3	1.578947368	0.00765317	0.735959185
GO:0007525~somatic muscle development	4	2.105263158	0.010369526	0.742072406
GO:0048800~antennal morphogenesis	3	1.578947368	0.014149556	0.77283168
GO:0045178~apical protein localization	3	1.578947368	0.016042131	0.753794947
GO:0007476~imaginal disc-derived wing morphogenesis	8	4.210526316	0.017484632	0.730273687
GO:0007422~peripheral nervous system development	5	2.631578947	0.019697357	0.725582829
GO:0048190~wing disc dorsal/ventral pattern formation	4	2.105263158	0.022111858	0.725254619
GO:0008362~chitin-based embryonic cuticle biosynthetic process	3	1.578947368	0.029439394	0.788564307
down-regulated genes (q<0.05)				
Term	Count	%	PValue	Bonferroni
GO:0042438~melanin biosynthetic process	3	1.648351648	0.013362355	0.996337704
GO:0048067~cuticle pigmentation	3	1.648351648	0.023261259	0.999945349
GO:0035179~larval turning behavior	2	1.098901099	0.035319345	0.999999692
GO:0048266~behavioral response to pain	2	1.098901099	0.035319345	0.999999692
GO:0007275~multicellular organism development	6	3.296703297	0.037732188	0.999999892
GO:0030717~karyosome formation	3	1.648351648	0.037992102	0.999999903
GO:0007268~chemical synaptic transmission	4	2.197802198	0.043931146	0.999999993
GO:0042742~defense response to bacterium	4	2.197802198	0.045602884	0.999999996
GO:0050966~detection of mechanical stimulus involved in sensory perception of pain	2	1.098901099	0.04681513	0.999999998
GO:0055085~transmembrane transport	8	4.395604396	0.058208559	1

Fig. S11. Transcriptome analysis of WD following caspase inhibition. To characterize the molecular mechanisms downstream of caspase activation, we determined the caspase inhibition-related changes in the overall transcriptome. We conducted a microarray analysis to detect the changes in gene expression upon *p35* overexpression in the WDs using *C10-Gal4*. We prepared two control conditions of *GFP* overexpressing and *LacZ* overexpressing WDs. Principal component analysis (PCA) segregated *p35* group with two control groups by PC1 and PC4 (A, B). Using the identified differentially expressed genes (C), we conducted a Gene Ontology (GO) analysis using DAVID (24, 25). While caspase activity is sometimes reported as a regulator of cell cycle (29, 30) or modulator of the Hippo signaling pathway (31), we found neither Hippo signaling nor cell cycle in the GO analysis (D). Our data imply that, at least in the WD, caspase inhibition affects overall transcriptome, but does not have major effect on tissue growth signaling pathway. These results suggest an alternative pathway for sustaining the tissue growth of WD. (A) Variance of principal components. (B) PCA biplot with samples plotted in two dimensions with projections to PC1 (x-axis) and PC4 (y-axis). Black circles, control (*C10* > *GFP* and *C10* > *LacZ*); red circles, caspase inhibition (*C10* > *p35*). (C) Top 25 differentially up-regulated/down-regulated genes in caspase-inhibited WD. (D) Top 10 GO terms from GO analysis of the dataset of genes with $q < 0.05$ differentially up-regulated/down-regulated on *p35* overexpression.

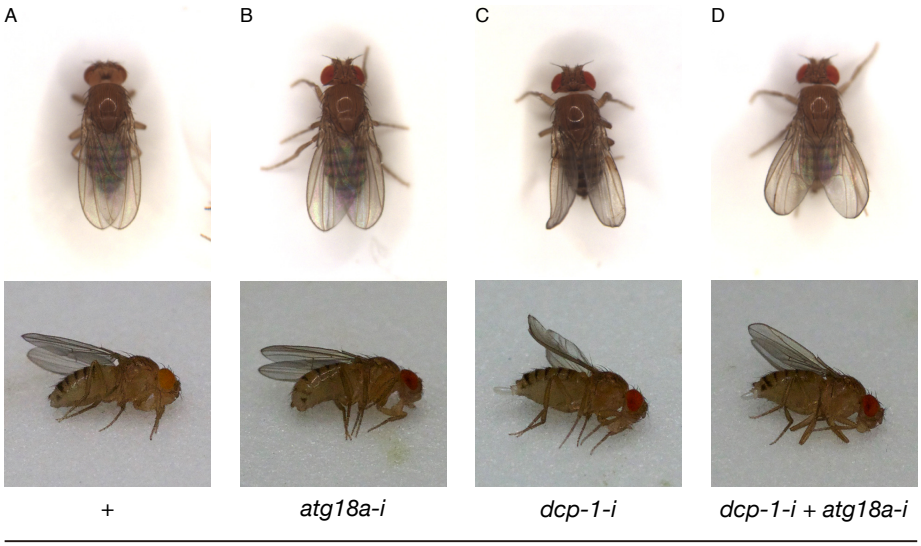

E

ap > mCD8::GFP				
Target Gene	Line ID	Control	*dcp-1-i* (V107560)	*decay-i* (V100168)
LacZ		Normal	Strongly Curled	Curled
atg3	V101364	Normal	Strongly Curled	Curled
atg18a	BL28061	Normal	Weakly Curled	Normal
atg7	V27432	Normal	Curled	Weakly Curled
	V45558	Normal	Strongly Curled	Curled
	V45560	Normal	Strongly Curled	Curled
	V45561	Normal	Strongly Curled	Curled
atg9	V10045	Normal	Curled	Weakly Curled
	V330100	Curled Downward	Strongly Curled	Normal
atg13	V27955	Normal	Curled	Weakly Curled
	V27956	Normal	Curled	Weakly Curled

Fig. S12. Knockdown of several autophagy-related genes rescues the curly-up wing phenotype. (A-D) Representative images of adult female flies. Top panel, top view; bottom panel, side view. *ap > mCD8::GFP* (A), *ap > mCD8::GFP, atg18a-i* (B), *ap > mCD8::GFP, dcp-1-i*^{V107560} (C), *ap > mCD8::GFP, dcp-1-i*^{V107560}*, atg18a-i* (D). (E) Table for the screening result. Dark red, Strongly Curled wing; red, Curled wing; pale red, Weakly Curled wing; blue, Downward curly wing.

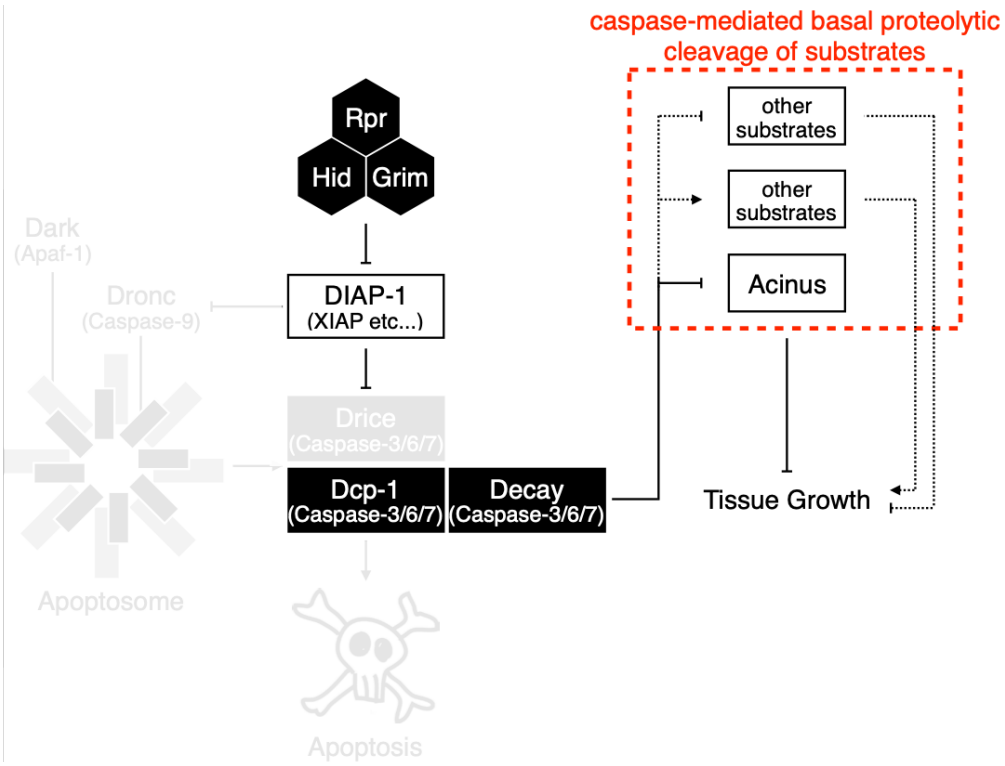

Fig. S13. Schematic model. Non-dying cells have Dronc-independent basal executioner caspase activity that mediates basal proteolytic cleavage of substrates, which sustains imaginal tissue growth.

References for SI

1. Klaiman G, Champagne N, LeBlanc AC (2009) Self-activation of Caspase-6 in vitro and in vivo: Caspase-6 activation does not induce cell death in HEK293T cells. *Biochim Biophys Acta - Mol Cell Res* 1793(3):592–601.

2. Wang XJ, et al. (2010) Crystal structures of human caspase 6 reveal a new mechanism for intramolecular cleavage self-activation. *EMBO Rep* 11(11):841–847.

3. Dagbay KB, Hardy JA (2017) Multiple proteolytic events in caspase-6 self-activation impact conformations of discrete structural regions. *Proc Natl Acad Sci* 114(38):E7977–E7986.

4. Kale A, Li W, Lee CH, Baker NE (2015) Apoptotic mechanisms during competition of ribosomal protein mutant cells: Roles of the initiator caspases Dronc and Dream/Strica. *Cell Death Differ* 22(8):1300–1312.

5. Kamber Kaya HE, Ditzel M, Meier P, Bergmann A (2017) An inhibitory mono-ubiquitylation of the Drosophila initiator caspase Dronc functions in both apoptotic and non-apoptotic pathways. *PLoS Genet* 13(2):e1006438.

6. Shen X, et al. (2016) Glioma-induced inhibition of caspase-3 in microglia promotes a tumor-supportive phenotype. *Nat Immunol* 17(11):1282–1290.

7. Allan LA., Clarke PR (2007) Phosphorylation of Caspase-9 by CDK1/Cyclin B1 Protects Mitotic Cells against Apoptosis. *Mol Cell* 26(2):301–310.

8. Nutt LK, et al. (2005) Metabolic regulation of oocyte cell death through the CaMKII-mediated phosphorylation of caspase-2. *Cell* 123(1):89–103.

9. Secinaro MA, et al. (2018) Glycolysis promotes caspase-3 activation in lipid rafts in T cells article. *Cell Death Dis* 9(2).

10. Zamaraev A V., Kopeina GS, Prokhorova EA, Zhivotovsky B, Lavrik IN (2017) Post-translational Modification of Caspases: The Other Side of Apoptosis Regulation. *Trends Cell Biol* 27(5):322–339.

11. Hayashi R, Handler D, Ish-Horowicz D, Brennecke J (2014) The exon junction complex is required for definition and excision of neighboring introns in Drosophila. *Genes Dev* 28(16):1772–1785.

12. Haberman AS, Akbar MA, Ray S, Krämer H (2010) Drosophila acinus encodes a novel regulator of endocytic and autophagic trafficking. *Development* 137(13):2157–2166.

13. Nandi N, Tyra LK, Stenesen D, Krämer H (2014) Acinus integrates AKT1 and subapoptotic caspase activities to regulate basal autophagy. *J Cell Biol* 207(2):253–268.

14. O'Farrell F, Wang S, Katheder N, Rusten TE, Samakovlis C (2013) Two-Tiered Control of Epithelial Growth and Autophagy by the Insulin Receptor and the Ret-Like Receptor, Stitcher. *PLoS Biol* 11(7):e1001612.

15. Scott RC, Juhász G, Neufeld TP (2007) Direct Induction of Autophagy by Atg1 Inhibits Cell Growth and Induces Apoptotic Cell Death. *Curr Biol* 17(1):1–11.

16. Williams DW, Kondo S, Krzyzanowska A, Hiromi Y, Truman JW (2006) Local caspase activity directs engulfment of dendrites during pruning. *Nat Neurosci* 9(10):1234–1236.

17. Kanuka H, et al. (2005) Drosophila caspase transduces Shaggy/GSK-3β kinase activity in neural precursor development. *EMBO J* 24(21):3793–3806.

18. Nakajima YI, Kuranaga E, Sugimura K, Miyawaki A, Miura M (2011) Nonautonomous Apoptosis Is Triggered by Local Cell Cycle Progression during Epithelial Replacement in Drosophila. *Mol Cell Biol* 31(12):2499–2512.

19. Kondo S, Senoo-Matsuda N, Hiromi Y, Miura M (2006) DRONC Coordinates Cell Death and Compensatory Proliferation. *Mol Cell Biol* 26(19):7258–7268.

20. Ren X, et al. (2013) Optimized gene editing technology for Drosophila melanogaster using germ line-specific Cas9. *Proc Natl Acad Sci U S A* 110(47):19012–19017.

21. Bolatto C, Parada C, Colmenares V (2017) A Rapid and Efficient Method to Dissect Pupal Wings of Drosophila Suitable for Immunodetections or PCR Assays. *J Vis Exp* (130):e55854.

22. Smyth GK (2004) Linear Models and Empirical Bayes Methods for Assessing Differential Expression in Microarray Experiments. *Stat Appl Genet Mol Biol* 3(1):1544-6115.

23. Smyth GK, Speed T (2003) Normalization of cDNA microarray data. *Methods* 31(4):265–273.

24. Huang DW, Sherman BT, Lempicki RA (2009) Bioinformatics enrichment tools: Paths toward the comprehensive functional analysis of large gene lists. *Nucleic Acids Res* 37(1):1–13.

25. Huang DW, Sherman BT, Lempicki RA (2009) Systematic and integrative analysis of large gene lists using DAVID Bioinformatics Resources. *Nat Protoc* 4(11):44–57.

26. Parker NF, Shingleton AW (2011) The coordination of growth among Drosophila organs in response to localized growth-perturbation. *Dev Biol* 357(2):318–325.

27. Shingleton AW (2011) The regulation of organ size in Drosophila. *Organogenesis* 6(2):76–87.

28. Obata F, et al. (2014) Necrosis-Driven Systemic Immune Response Alters SAM Metabolism through the FOXO-GNMT Axis. *Cell Rep* 7(3):821–833.

29. Hashimoto T, Yamauchi L, Hunter T, Kikkawa U, Kamada S (2008) Possible involvement of caspase-7 in cell cycle progression at mitosis. *Genes to Cells* 13(6):609–621.

30. Hashimoto T, Kikkawa U, Kamada S (2011) Contribution of Caspase(s) to the Cell Cycle Regulation at Mitotic Phase. *PLoS One* 6(3):e18449.

31. Yosefzon Y, et al. (2018) Caspase-3 Regulates YAP-Dependent Cell Proliferation and Organ Size. *Mol Cell* 70(4):573-587.